

11-20-2003

# Twin-Rainbow Metrology. I. Measurement of the Thickness of a Thin Liquid Film Draining Under Gravity

Charles L. Adler

James A. Lock  
Cleveland State University, j.lock@csuohio.edu

Ian P. Rafferty

Wayne Hickok

Follow this and additional works at: [https://engagedscholarship.csuohio.edu/sciphysics\\_facpub](https://engagedscholarship.csuohio.edu/sciphysics_facpub)

 Part of the [Physics Commons](#)

**How does access to this work benefit you? Let us know!**

## *Publisher's Statement*

This paper was published in Applied Optics and is made available as an electronic reprint with the permission of OSA. The paper can be found at the following URL on the OSA website: <http://www.opticsinfobase.org/ao/abstract.cfm?URI=ao-42-33-6584>. Systematic or multiple reproduction or distribution to multiple locations via electronic or other means is prohibited and is subject to penalties under law.

## Original Citation

Adler, Charles L.; Lock, James A.; Rafferty, Ian P.; and Hickok, Wayne. "Twin-Rainbow Metrology. I. Measurement of the Thickness of a Thin Liquid Film Draining Under Gravity." *Applied Optics* 42 (2003): 6584-6594.

## Repository Citation

Adler, Charles L.; Lock, James A.; Rafferty, Ian P.; and Hickok, Wayne. "Twin-Rainbow Metrology. I. Measurement of the Thickness of a Thin Liquid Film Draining Under Gravity" (2003). *Physics Faculty Publications*. 97.  
[https://engagedscholarship.csuohio.edu/sciphysics\\_facpub/97](https://engagedscholarship.csuohio.edu/sciphysics_facpub/97)

This Article is brought to you for free and open access by the Physics Department at EngagedScholarship@CSU. It has been accepted for inclusion in Physics Faculty Publications by an authorized administrator of EngagedScholarship@CSU. For more information, please contact [library.es@csuohio.edu](mailto:library.es@csuohio.edu).

# Twin-rainbow metrology. I. Measurement of the thickness of a thin liquid film draining under gravity

Charles L. Adler, James A. Lock, Ian P. Rafferty, and Wayne Hickok

We describe twin-rainbow metrology, a new optical technique used to measure the thickness of thin films in a cylindrical geometry. We also present an application of the technique: measurement of the thickness of a Newtonian fluid draining under gravity. We compare these measurements with fluid mechanics models. © 2003 Optical Society of America

*OCIS codes:* 290.3200, 120.0120.

## 1. Introduction

Rainbow refractometry is the name given to a collection of optical techniques used to determine the index of refraction and the cross-sectional shape of large, transparent scatterers that possess near-circular cross sections by determination of the position and interference structure of rainbow caustics of light scattered by them. The rainbow caustic is an attractive feature to use in inverse scattering for several reasons. Its brightness is often orders of magnitude higher than other features of the scattered light. It is structurally stable, i.e., limited distortions of the shape of the scatterer do not destroy the rainbow but only change its position. It also has a simple interpretation in terms of geometrical optics as a local extremum in the scattering angle as a function of the light ray impact parameter. Rainbow refractometry has been used to measure the temperature of fuel droplets, the index of refraction of liquids, and the exact cross-sectional shape of dielectric cylinders.<sup>1-7</sup> This is the first in a series of papers in which we describe the capabilities of twin-rainbow metrology (TRM), a new optical technique based on rainbow refractometry, that allows the measurement of the thicknesses of thin films in cylindrical geometries to

sub-micrometer resolution. The technique can be used under the following conditions:

- (1) The film must lie on the surface of a cylinder with a circular cross section. The film thickness should be radially uniform, although in general it will vary along the length of the cylinder.
- (2) The cylinder and film should be reasonably transparent at the probe wavelength.
- (3) The real part of the index of refraction of the coating and cylinder at the probe wavelength must be accurately known and differ by at least 0.05.

TRM is applicable for film thicknesses in the range from roughly 0.1  $\mu\text{m}$  to over 100  $\mu\text{m}$  and, unlike conventional microphotographic techniques, allows the measurement over a wide field of view. The technique is also high speed, limited only by the capture rate of the camera used to record the twin rainbows. The way in which TRM is used depends on the film thickness. If the film is more than approximately 4  $\mu\text{m}$  thick, the angular position of one or both of a pair of twin primary rainbows produced by the film-coated cylinder are recorded, and the angular positions of the rainbows are used to determine the thin-film profile by the numerical quadrature of a differential equation. However, if the films are of the order of 4  $\mu\text{m}$  thick or less, the interference of the overlapping twin rainbows is analyzed to measure the film profile.

In this paper we report our use of TRM to measure the thickness of a thin, Newtonian liquid film draining under the force of gravity in the so-called tail region of the film. (The tail of a draining fluid film is the top of the film, i.e. the region between the line of attachment of the fluid to the rod and a few millimeters above the bottom of the film; the head of the film

---

C. L. Adler (cladler@smcm.edu), I. P. Rafferty, and W. Hickok are with the Department of Physics, St. Mary's College of Maryland, 18952 East Fisher Road, St. Mary's City, Maryland 20686. J. A. Lock is with the Department of Physics, Cleveland State University, Cleveland, Ohio 44115.

Received 24 January 2003; revised manuscript received 11 June 2003.

0003-6935/03/336584-11\$15.00/0

© 2003 Optical Society of America

is the bottom few millimeters.) We chose this system because it allowed us to easily vary the film thickness by 2 orders of magnitude and to vary other experimental parameters (such as fluid viscosity) by changing the liquid used in the experiment. In addition, the film thickness in the tail is well modeled by the Jeffreys parabola (discussed in Subsection 3.B), which can be used as a check of our experimental technique. One point that we discuss at greater length is that, although these solutions are well known, to our knowledge there are relatively few accurate experimental measurements that have checked them. Other extensions of this research are discussed in the conclusions and in later papers in this series.

## 2. Theory of the Coated Cylinder Rainbow

The origin of the rainbows created by a transparent cylinder with a circular cross section in the context of ray theory is as follows. Parallel light rays are refracted into the cylinder, internally reflect ( $p - 1$ ) times, and are refracted out. The deflection angle  $\Theta$  is a function of the angle of incidence  $\theta_i$  between the incident ray trajectory and the normal to the droplet surface. At the angle  $\theta_i^R$ , the deflection angle  $\Theta$  has an extremal value. For the  $(p - 1)$ th-order rainbow, we have

$$\cos \theta_i^R = \left( \frac{n^2 - 1}{p^2 - 1} \right)^{1/2}, \quad (1)$$

and the deflection angle is

$$\Theta^R = 2\theta_i^R + (p - 1)\pi - 2p\theta_t^R, \quad (2)$$

where the angle  $\theta_t^R$  is the refracted angle of the rainbow ray inside the droplet:

$$\sin \theta_t^R = \frac{\sin \theta_i^R}{n} = \left[ \frac{(p/n)^2 - 1}{p^2 - 1} \right]^{1/2}. \quad (3)$$

For the first-order ( $p = 2$ ) rainbow, the deflection angle  $\Theta^R$  and the scattering angle  $\theta^R$  are identical. The Debye-series expansion of the Rayleigh solution for scattering of a normally incident plane wave by a cylinder confirms the ray theory results when the radius of the cylinder is large compared to the wavelength of light.<sup>8</sup>

For typical rainbow refractometry applications, such as particle temperature measurement, one often deals with particles that are either aspherical or have an inhomogeneous index of refraction (or both).<sup>6,9-13</sup> The simplest case of index inhomogeneity is rainbow scattering by a coated sphere or cylinder. The core has refractive index  $n_1$ , and the coating, which completely surrounds the core, has index  $n_2$ . Figure 1 shows the geometry that we are considering. Here  $r$  is the thickness of the coating on the cylinder, and  $a$  is the core radius. Because of the two possible one internal reflection ray paths shown in Fig. 1, there are two separate minima in the scattering angle, which we label  $\theta_\alpha^R$  and  $\theta_\beta^R$ —i.e., the coated sphere produces twin primary rainbows.

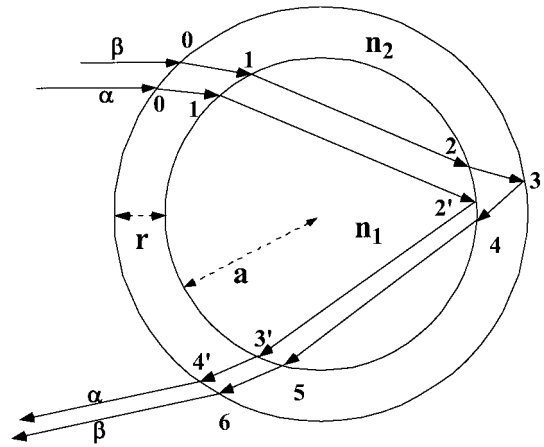


Fig. 1. Coated cylinder cross section and the trajectory of the twin-rainbow rays.

The angles of the rainbows are functions of the relative thickness of the coating  $r/a$  and the refractive indices of the core and coating. In Ref.14 the authors derived an approximate formula for  $\theta_\alpha^R$  and  $\theta_\beta^R$ , which is correct to first order in  $r/a$ . If  $\theta^R$  is the scattering angle of the primary rainbow of a homogeneous sphere or cylinder of index  $n_1$ , then the scattering angles of the twin rainbows are approximately<sup>13,14</sup>

$$\theta_\alpha^R = \theta^R + \frac{2r}{a} \left[ \left( \frac{4 - n_1^2}{3n_2^2 + n_1^2 - 4} \right)^{1/2} - \left( \frac{4 - n_1^2}{n_1^2 - 1} \right)^{1/2} \right], \quad (4a)$$

$$\theta_\beta^R = \theta^R + \frac{2r}{a} \left[ 2 \left( \frac{4 - n_1^2}{3n_2^2 + n_1^2 - 4} \right)^{1/2} - \left( \frac{4 - n_1^2}{n_1^2 - 1} \right)^{1/2} \right]. \quad (4b)$$

This derivation is based on a Taylor-series expansion of the rainbow angles derived from ray theory and was checked by the Aden-Kerker extension of Mie theory for a coated sphere.<sup>15</sup>

The semiclassical theory of rainbow scattering that takes into account the wave nature of light is Airy theory.<sup>16-18</sup> The assumption behind the Airy theory is that the phase front of the light wave exiting near the rainbow angle is cubic, and the amplitude of the electromagnetic field is slowly varying. This is an excellent approximation for the size parameter  $X = 2\pi a/\lambda \sim 2000$  or larger, although one must appeal to Mie theory for its justification.<sup>8,19</sup> If we define the Airy integral as

$$\text{Ai}(-w) = \frac{3^{1/3}}{\pi} \int_0^\infty \cos(t^3 - 3^{1/3}wt)dt, \quad (5)$$

the Fraunhofer diffracting the cubic phase into the far field yields

$$E(\theta) \sim \text{Ai} \left[ - \frac{X^{2/3}}{h^{1/3}} (\theta - \theta^R) \right], \quad (6)$$

where  $\theta$  is the scattering angle and

$$h = \frac{9(4 - n_1^2)^{1/2}}{4(n_1^2 - 1)^{3/2}} \quad (7)$$

is a dimensionless measure of the phase-front curvature.<sup>20</sup> Properties of the Airy integral can be found in Ref. 21.

To find the interference pattern from the overlap of the twin rainbows, we must also take into account a phase shift between the two rainbow rays that are proportional to the film thickness. The phase shift arises from two causes: First, the ray corresponding to the  $\beta$  rainbow travels a longer distance than that of the  $\alpha$  rainbow as it refracts into the coating before reflecting back (see Fig. 1); second, the  $\alpha$  and  $\beta$  rainbow rays exit the droplet at slightly different points. From this, the intensity of the scattered light in the far field is

$$\begin{aligned} I(\theta) = & I_1 \text{Ai} \left[ -\frac{X^{2/3}}{h^{1/3}} (\theta - \theta_\alpha^R) \right]^2 \\ & + I_2 \text{Ai} \left[ -\frac{X^{2/3}}{h^{1/3}} (\theta - \theta_\beta^R) \right]^2 \\ & + 2(I_1 I_2)^{1/2} \text{Ai} \left[ -\frac{X^{2/3}}{h^{1/3}} (\theta - \theta_\alpha^R) \right] \\ & \times \text{Ai} \left[ -\frac{X^{2/3}}{h^{1/3}} (\theta - \theta_\beta^R) \right] \\ & \times \cos \left[ \frac{4\pi r}{\lambda} \left( \frac{3n_2^2 + n_1^2 - 4}{3} \right)^{1/2} \right], \quad (8) \end{aligned}$$

where  $I_1$  is the intensity of the  $\alpha$  rainbow in the absence of the  $\beta$  rainbow and  $I_2$  is the intensity of the  $\beta$  rainbow in the absence of the  $\alpha$  rainbow. The ratio  $I_2/I_1$  is obtained by use of flat-surface Fresnel coefficients. For  $n_1 = 1.61$  and  $n_2 = 1.40$ , one finds  $I_2/I_1 \sim 30$ .

The concept outlined above is the basis of TRM: If a cylinder is coated with a radially uniform thin film and a laser beam is incident on the cylinder, the angular position of the twin primary rainbows can be used to determine the thickness of the thin-film coating. For very thin films, one can measure the coating thickness using interference of the overlapping twin rainbows.

### 3. Experiment

To test the utility of TRM, we used the technique to measure the thickness of thin liquid films draining under the force of gravity. This is an almost ideal system for these measurements because the coating thickness varies over time by 2 orders of magnitude during the course of an experiment, enabling us to test TRM over a wide variety of length scales. Fluid parameters such as refractive index, density, and viscosity are well known and can be varied enormously, and there is a well-established theory for the shape of the thin film as a function of time that can be tested to high precision.

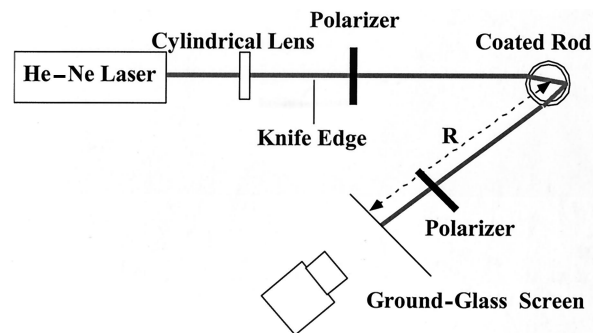


Fig. 2. Experimental setup for twin-rainbow metrology.

#### A. Apparatus

Our experimental apparatus is shown in Fig. 2. The beam from a He-Ne laser is expanded vertically by use of a cylindrical lens and was incident on a vertical glass rod near the primary rainbow impact parameter. The twin first-order rainbows were projected onto a ground-glass screen and imaged with a video camera and frame grabber. Two polarizing filters were used. The first was set to ensure that the light incident on the rod was polarized vertically, and the second was placed in front of the camera to control the intensity incident on it. The glass rod itself was specially manufactured by Collimated Holes, Inc. to have a nearly circular cross section and uniform index of refraction. The cylinder radius is  $a = 0.316 \pm 0.01$  cm, and its refractive index is  $n_1 = 1.6147 \pm 0.002$ . The measurement of the cylinder's index of refraction was made by rainbow refractometry as described in Ref. 6; the uncertainty quoted is based on a curve fit of the angular position of the primary rainbow as a function of rod orientation to the two-half-ellipse model developed in that paper.

To perform an experiment, a cup filled with Corning 200 Silicone Oil was raised over the bottom of the rod to a height of 2.3 cm. Once the cup was removed and the oil-coated rod was illuminated by the laser beam, the twin rainbows from this section of the rod were recorded by the video camera. Corning 200 Silicone Oil is available in a wide range of viscosities. In our experiments, we used fluids with kinematic viscosities ranging from 0.015 to over 10 cm<sup>2</sup>/s, a range of 3 orders of magnitude. [In this paper we always refer to the kinematic viscosity, which is the fluid viscosity divided by the fluid density (0.97 g/cm<sup>3</sup>)]. Because of the wide range of viscosities used, the total duration of an experiment varied from less than a minute for the least viscous to over 6 h for the most viscous fluids. Although the lowest-viscosity fluids we used are somewhat volatile, we did not attempt to control for evaporation during the course of these experiments; however, we do not believe that evaporation was a significant factor in these experiments. We discuss this point in more detail in Section 5. The refractive index of the fluid varied from  $1.38 \pm 0.01$  for the low-viscosity fluids to  $1.40 \pm 0.01$  for the high-viscosity fluids. The refractive index of the fluid was measured by rainbow re-

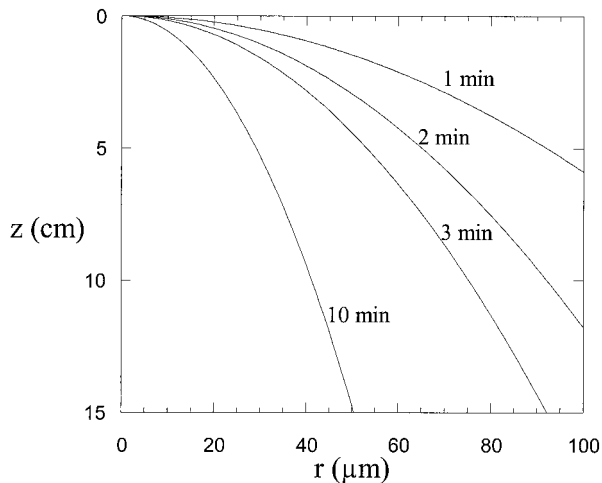


Fig. 3. Theoretical profile of a draining thin film as a function of time for  $\mu = 12 \text{ cm}^2/\text{s}$ . Note the different scales for the  $r$  and  $z$  axes.

fractometry performed on a pendant droplet; the uncertainties quoted reflect the predicted accuracy of the rainbow refractometry setup we used for the measurement and are not based on a standard deviation taken from repeated measurements. However, they match values quoted for the refractive indices by Corning.

#### B. Jeffreys Parabola for Draining Fluids

The analysis of these experiments relies on a theoretical knowledge of the shape of the thin film as a function of time. The shape of a thin film draining under gravity down an infinite vertical plate was first derived by Jeffreys:

$$z = \left(\frac{g}{\mu}\right) r^2 t, \quad (9)$$

where  $z$  is the vertical distance (down) from the top of the thin film,  $r$  is its thickness,  $g$  is the acceleration of gravity, and  $\mu$  is the kinematic viscosity of the liquid.<sup>22</sup> Figure 3 shows a theoretical profile of a thin liquid film at several different times for a kinematic viscosity  $\mu = 12 \text{ cm}^2/\text{s}$ . Note that the  $r$  and  $z$  scales differ by over 2 orders of magnitude and that the contact point of the fluid with the rod remains fixed. Equation (9) is valid for drainage from a cylinder when<sup>23–25</sup> the thickness of the thin film is much smaller than the cylinder radius, effects that are due to surface tension are unimportant, and when the influence of any boundaries such as the bottom of the rod can be ignored. For these reasons, the Jeffreys parabola solution is valid for values of  $z$  ranging from roughly 1 mm below the top of the film (the point of attachment or contact line), above which effects that are due to surface tension are important, to 3–4 mm above the bottom of the rod.<sup>24</sup> In the regime where the Jeffreys solution is valid, the shape of the thin film should be close to a parabola that thins over time.

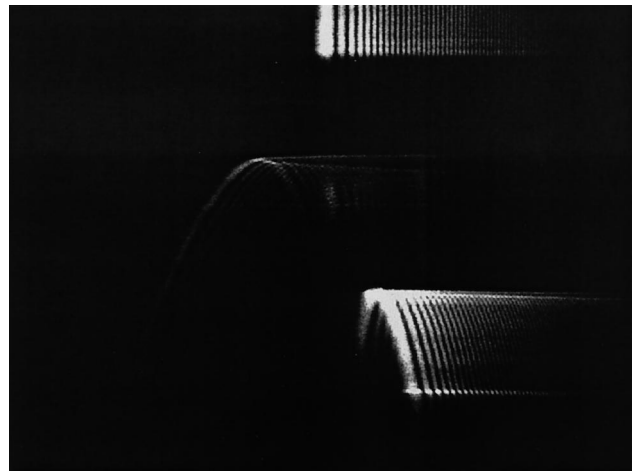


Fig. 4. Video image of twin rainbows for  $\mu = 0.015 \text{ cm}^2/\text{s}$  and  $t = 10 \text{ s}$ .

## 4. Results

### A. Rainbow Gap

Figure 4 shows a frame from a video of the twin rainbows produced by a thin film of silicone oil with kinematic viscosity  $\mu = 0.015 \text{ cm}^2/\text{s}$  at a time  $t = 10 \text{ s}$ . The twin rainbows are clearly visible in the lower two thirds of the picture. The  $\alpha$  rainbow is the dimmer bow because the core–coating internal reflection is weaker than the internal reflection at the air–coating interface responsible for the  $\beta$  rainbow. Above the point of attachment, the straight fringes of the rainbow that are due to the uncoated rod are clearly visible. The picture has two surprising features: The  $\alpha$  and  $\beta$  rainbows are curved over in the vertical direction, and there is a vertical gap between the top of each rainbow and the point of attachment. The gap width is different for each rainbow and was observed to decrease slowly over time. We call the vertical coordinate of the twin rainbows on the ground-glass screen  $Z_\alpha$  and  $Z_\beta$ , respectively. The gap width is the distance from the point of attachment to the maximum value of these coordinates,  $Z_\alpha^0$  and  $Z_\beta^0$ . Graphs of  $Z_\alpha^0$  and  $Z_\beta^0$  as a function of time for fluids of several different viscosities are shown in Figs. 5(a) and 5(b).

The reason the gap exists is as follows. Because the surface of the silicone oil film is not vertical, an incoming light ray is deflected vertically downward because of refraction and reflection at the air–coating and coating–core interfaces. If the slope of the film is nearly vertical (i.e.,  $dz/dr \gg 1$ ), a light ray incident on the rod a distance  $z$  below the point of attachment will be deflected vertically to a point  $Z_\alpha$  or  $Z_\beta$  on the screen:

$$Z_{\alpha,\beta} = z \left( 1 + \frac{R}{L_f} \right) + \frac{\gamma_{\alpha,\beta} R}{dz/dr}, \quad (10)$$

where  $R$  is the distance from the center of the rod to the screen, and  $\gamma_{\alpha,\beta}$  are constants that depend only on the refractive indices of the core and coating. The

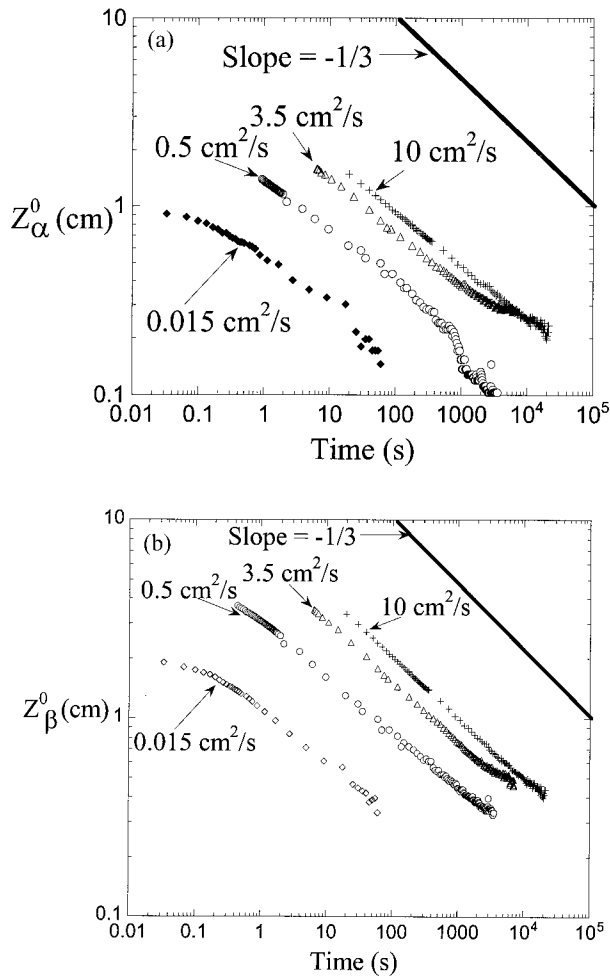


Fig. 5. (a)  $\alpha$  rainbow gap width  $Z_{\alpha}^0(t)$  as a function of time for several different viscosity silicone oils. (b)  $\beta$  rainbow gap width  $Z_{\beta}^0(t)$  as a function of time for several different viscosity silicone oils.

notations  $\gamma_{\alpha,\beta}$  and  $Z_{\alpha,\beta}$  are used to refer to each of the twin rainbows, respectively. The quantities  $\gamma_{\alpha}$  and  $\gamma_{\beta}$  differ, as do the gap widths for each of the rainbows, because of the difference in the ray paths of the light making up each bow.  $L_f$  is the distance from the focal point of the cylindrical lens to the rod. The factor  $R/L_f$  in Eq. (10) is necessary because the beam is expanding as it is scattered from the rod to the screen. In Appendix A we show that

$$\gamma_{\alpha} = \frac{2}{3^{1/2}} [(3n_2^2 + n_1^2 - 4)^{1/2} - (n_1^2 - 1)^{1/2}], \quad (11a)$$

$$\gamma_{\beta} = \frac{2}{3^{1/2}} [2(3n_2^2 + n_1^2 - 4)^{1/2} - (n_1^2 - 1)^{1/2}]. \quad (11b)$$

For  $n_1 = 1.61$  and  $n_2 = 1.40$ ,  $\gamma_{\alpha} = 0.985$  and  $\gamma_{\beta} = 3.42$ .

Setting  $dZ_{\alpha,\beta}/dr = 0$  to find the gap width and using Eq. (9) for  $z(r)$ , we obtain

$$Z_{\alpha,\beta}^0(t) = \frac{3}{2} \left[ \gamma_{\alpha,\beta}^2 R^2 \left( 1 + \frac{R}{L_f} \right) \right]^{1/3} \left( \frac{\mu}{2gt} \right)^{1/3}. \quad (12)$$

Table 1. Power-Law Scaling Coefficients  $A_{\alpha,\beta}$  for the Rainbow Gap<sup>a</sup>

$\mu$ (cm <sup>2</sup> /s)	$A_{\alpha}$ (theory) (cm s <sup>1/3</sup> )	$A_{\alpha}$ (experiment) (cm s <sup>1/3</sup> )	$A_{\beta}$ (theory) (cm s <sup>1/3</sup> )	$A_{\beta}$ (experiment) (cm s <sup>1/3</sup> )
0.015	0.442	0.442	0.92	1.02
0.5	1.42	1.42	3.27	2.82
3.5	2.72	2.92	6.26	6.66
10	3.86	3.98	8.88	9.04
11 (theory only)	3.98		9.17	

<sup>a</sup>Theoretical values for  $\mu = 11$  cm<sup>2</sup>/s are shown for comparison with the nominal  $\mu = 10$  cm<sup>2</sup>/s viscosity fluid.

A log-log plot of  $Z_{\alpha,\beta}^0(t)$  versus  $t$  should have a slope of  $-1/3$ . In practice, there is a correction factor to Eq. (12) because it was derived from geometrical optics. In our experiments, the gap width is measured from the peak of the primary rainbow main fringe, which is shifted slightly from the Descartes position of the rainbow as predicted by geometrical optics. This will add a constant offset to Eq. (12). To examine our data we performed a least-squares fit of  $Z_{\alpha,\beta}^0(t)$  to the function

$$Z_{\alpha,\beta}^0(t) = A_{\alpha,\beta} t^{-1/3} + B_{\alpha,\beta}. \quad (13)$$

The constant offset  $B_{\alpha,\beta}$  should be of the order of  $R/X^{23} \sim 0.05$  cm. From our experimental data,  $B_{\alpha,\beta}$  was always found to be between 0.07 and 0.16 cm. This variation in  $B_{\alpha,\beta}$  is due to two effects: First, it is difficult to determine the exact position of the peak of the primary rainbow fringe (in practice this was harder to do for the  $\beta$  rainbow because the images of the  $\beta$  rainbow were often saturated), and second the fringe spacings of the supernumerary rainbows of a glass rod have large fluctuations as a function of the rod's orientation.<sup>7</sup> Because the rod was removed and cleaned between trials, the orientation is random, leading to variation in  $B_{\alpha,\beta}$ .

It can be seen from Figs. 5(a) and 5(b) that the  $t^{1/3}$  scaling law seems to be violated at short times for the lowest-viscosity fluid. This is an artifact arising from the way in which the data were taken. It takes roughly 0.2 s to remove the silicone oil container when the experiment is started. Because of this, the exact time from release is approximately 0.2 s earlier than indicated in Fig. 5. This is unimportant for high-viscosity fluids, as we did not begin measuring the gap width until several seconds into the experiment. However, it is important for the  $\mu = 0.015$  cm<sup>2</sup>/s viscosity fluid. When determining  $A$  for this fluid, we eliminated all data earlier than  $t = 0.3$  s.

Values for  $A_{\alpha,\beta}$  in Eq. (12) were determined for the fluids and compared with theoretical predictions based on the nominal viscosity of the fluid. The results are summarized in Table 1. As can be seen, the comparison between theory and experiment is quite good.

#### B. Inversion of Experimental Data

We now turn to the question of how the shape of the film profile can be determined directly from the scat-

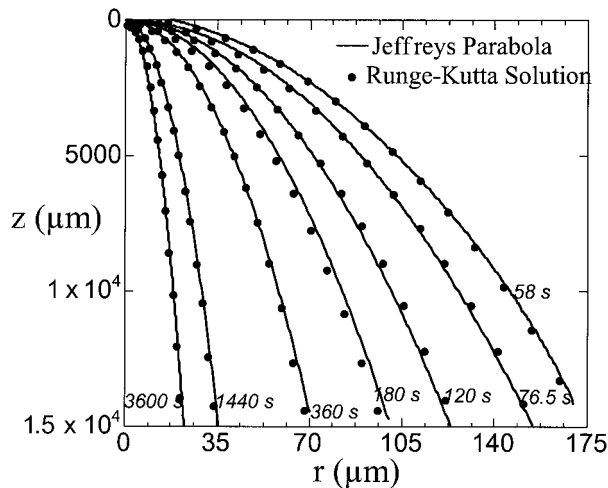


Fig. 6. Comparison of inverted TRM data (solid curves) to predictions made by the Jeffreys theory (filled circles). Data were taken from the  $\alpha$  rainbow for  $\mu = 10 \text{ cm}^2/\text{s}$  nominal viscosity. The best-fit viscosity to the data is  $\mu = 12 \text{ cm}^2/\text{s}$ .

tering data. We wish to determine  $z(r)$  knowing  $Z_{\alpha,\beta}(\theta_{\alpha,\beta}^R)$ . To do this inversion we must use Eq. (10) to invert  $Z_{\alpha,\beta}$  to find  $z$ . Because the film thickness changes with  $z$ , the position of the rainbow ray on the viewing screen,  $Z_{\alpha,\beta}$ , is not proportional to  $z$ ; and we find the determination of  $r(z)$  more complicated than merely measuring  $\theta_{\alpha,\beta}^R$  as a function of  $Z_{\alpha,\beta}$  and using Eqs. (4a) and (4b). We can rewrite Eq. (10) as

$$\frac{dz}{dr} = \frac{\gamma_{\alpha,\beta} R}{Z_{\alpha,\beta}(r) - (1 + R/L_f)z}. \quad (14)$$

From Eqs. (4a) and (4b), the angular separation of either rainbow from the position of the rainbow that is due to the uncoated rod is proportional to  $r$ . So we can obtain  $Z_{\alpha,\beta}(r)$  by digitizing the video image and then determine  $z(r)$  by numerically integrating the differential equation using the data from the digitized image. When determining  $Z_{\alpha,\beta}(r)$  we subtract off the constant offset  $B_{\alpha,\beta}$  found from the gap data. We use the boundary condition

$$\lim_{r \rightarrow \infty} z(r) = \frac{Z_{\alpha,\beta}(r)}{1 + R/L_f}, \quad (15)$$

corresponding to the asymptotically vertical film surface far below the contact line and integrate from high  $r$  downwards. It is important to integrate this way as Eq. (14) is numerically unstable when integrated from low  $r$  to high  $r$ .

Figure 6 shows several profiles of the fluid found from numerical integration of the differential equation by use of a fourth-order Runge–Kutta algorithm and comparison with the Jeffreys theory. In Fig. 6 the profiles were determined from the  $\alpha$  rainbow scattering data. Here the nominal kinematic viscosity of the fluid is  $\mu = 10 \text{ cm}^2/\text{s}$ , whereas the data is best fit with  $\mu = 12 \text{ cm}^2/\text{s}$ . By comparison, the  $A_{\alpha,\beta}$  coefficients determined from Eq. (12) for this fluid corre-

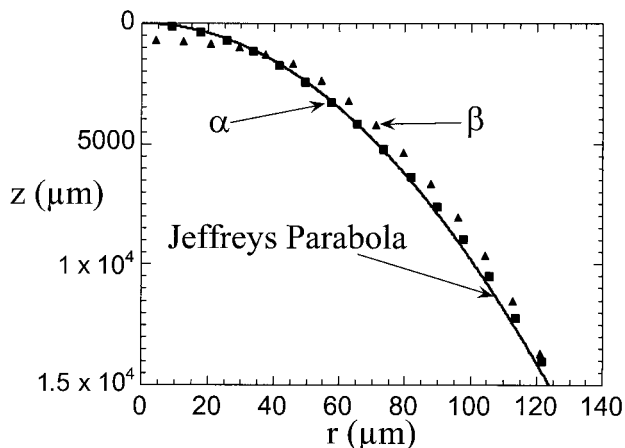


Fig. 7. Comparison of inverted TRM data for the  $\alpha$  (filled squares) and  $\beta$  rainbows (filled triangles) at  $t = 120 \text{ s}$ . The nominal viscosity for the fluid is  $\mu = 10 \text{ cm}^2/\text{s}$ . The best-fit viscosity to the data is  $\mu = 12 \text{ cm}^2/\text{s}$ .

spond to a viscosity of  $11 \text{ cm}^2/\text{s}$ . From this, it is clear that there is good agreement between the Jeffreys theory and our data. Figure 7 shows two profiles of the nominal  $\mu = 10 \text{ cm}^2/\text{s}$  fluid at time  $t = 120 \text{ s}$  that we found by inverting both the  $\alpha$  and the  $\beta$  rainbow scattering data. As expected, the two profiles are similar.

### C. Twin-Rainbow Interference

When the liquid film becomes sufficiently thin, the geometrical-optics model of Eqs. (4a) and (4b) is insufficient because of the overlap and interference of the twin-rainbow fringes. Interference becomes important when the angular separation of the two bows becomes comparable to the angular separation of the main peak to its first supernumerary; using Eqs. (4a), (4b), and approximation (6), we can estimate this as

$$r_{\text{int}} \sim \frac{a}{2} \left( \frac{3n_2^2 + n_1^2 - 4}{4 - n_1^2} \right)^{1/2} \frac{h^{1/3}}{X^{2/3}} \sim 3 \text{ } \mu\text{m}. \quad (16)$$

Figure 8 shows a frame from a video of the twin rainbows for a viscosity  $\mu = 0.015 \text{ cm}^2/\text{s}$  at time  $t = 45 \text{ s}$ . Only the region of the rainbows below the gaps

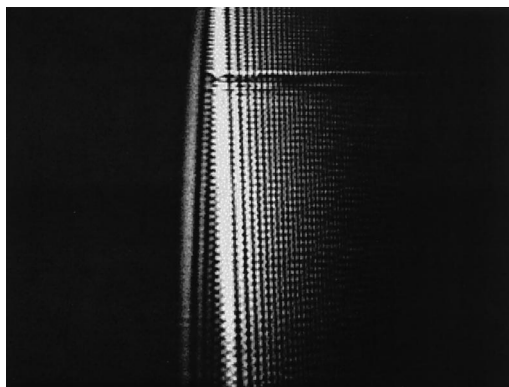


Fig. 8. Video image of the twin-rainbow interference pattern for  $\mu = 0.015 \text{ cm}^2/\text{s}$  and  $t = 45 \text{ s}$ .

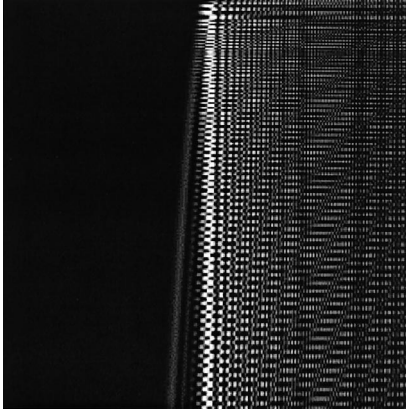


Fig. 9. Computer simulation of the twin-rainbow interference pattern of Fig. 8.

is shown this time to make Fig. 8 easier to understand. At this time a complex interference pattern as well as the hint of a moiré structure can be seen (compare with Fig. 4 where no interference structure is seen.) We can attempt to simulate this using Eq. (8) plus the Jeffreys theory [Eq. (9)]. The result is shown in Fig. 9. The overall structure of the experimental data and the theoretical model are similar.

The vertical checkerboard banding of the brighter  $\beta$  rainbow peak and the first few supernumeraries that can be seen in the structure are explained as follows. Imagine a ray incident on the cylinder at an impact parameter near the rainbow angle. On refracting into the coated rod, part of the light will internally reflect at the core–coating interface and part will reflect at the coating–air interface. On refraction out of the coated rod, the two exiting rays will be almost parallel and will interfere. The nature of the interference will depend on the thickness of the coating layer. Constructive interference will occur for coating thicknesses where the cosine term in Eq. (8) is positive, and destructive interference will occur where it is negative. As one moves down the rod, the change in the coating thickness with height gives alternating bright and dark fringes. From Eq. (8), the change in thickness to go from one bright fringe to the next is

$$\Delta r_b = \frac{\lambda}{2} \left( \frac{3}{3n_2^2 + n_1^2 - 4} \right)^{1/2} = 0.277 \text{ } \mu\text{m}. \quad (17)$$

We can determine  $\Delta r_b$  experimentally by examining a region of the rod where the interference pattern is visible and the twin rainbows are well resolved. We can then calculate the change in thickness between two vertically adjacent bright fringes by measuring the change in the angular separation of the twin rainbows. From this we find that  $\Delta r_b = 0.266 \pm 0.05 \text{ } \mu\text{m}$ .

The large standard deviation in the experimental determination of  $\Delta r_b$  deserves some comment. One issue that complicates this measurement is that the supernumerary rainbows are not regularly spaced. As the scattering angle increases from the

rainbow angle, their spatial frequency increases. Because two or more fringes of the  $\alpha$  rainbow overlap one fringe of the  $\beta$  rainbow and the relative phase of the light is reversed between adjacent supernumeraries, both constructive and destructive interference occur within the main peak of the  $\beta$  rainbow. The consequence of this is that the peak is split in two lobes. This complicates both the determination of the angular separation of the twin rainbows and the vertical separation of adjacent bright bands. This is also the reason the checkerboard pattern increases its spatial frequency as the scattering angle increases. In like manner, the interference structure on the first two supernumeraries of the  $\alpha$  rainbow is due to their interference with the complex ray of the  $\beta$  rainbow that extends into the classical shadow region.

In deriving Eq. (8), we ignored the vertical curvature of the twin rainbows produced by the parabolic shape of the surface of the film. This approximation is valid so long as  $dz/dr \gg 1$ , but a complete theory will have to include these curvature effects.

## 5. Enhancements of the Twin-Rainbow Metrology Technique

The main conclusion that we draw from the experiments reported in Section 4 is that TRM can be successfully used to measure the shape of a thin film in a cylindrical geometry. There are, however, a number of other related TRM experiments that should be discussed, which will be reported more completely in a forthcoming paper. For a Newtonian fluid draining off a cylinder, one can use TRM along with the presumed shape of the film to determine its viscosity to an accuracy of the order of a few percent or better. In our experiments, we noted the temperature of the room in which the experiments occurred ( $24 \text{ }^\circ\text{C} \pm 1 \text{ }^\circ\text{C}$  over the course of the study) but did not attempt to measure the fluid temperature or try to control it. We also used the nominal viscosity as given by the vendor in our theory, although we did measure the viscosity of the nominally  $0.015\text{-cm}^2/\text{s}$  fluid with an Ostwald viscometer and found a value of  $0.014 \pm 0.001 \text{ cm}^2/\text{s}$ . (The error indicated here is the standard deviation of three measurements.) We are currently planning a series of experiments with a commercial viscometer to check our results against it. We can measure viscosity by TRM in two separate ways: (1) by measuring the gap width as a function of time and comparing this with Eq. (11); or (2) by inverting the data to find the thin-film profile and comparing it with the Jeffreys parabola. We call these measurement techniques TRM viscometry.

All the fluids used in the experiments discussed here are Newtonian fluids, i.e., ones in which the shear rate is proportional to the shear stress. We are also beginning a series of experiments to determine the shape of a draining non-Newtonian fluid. We are investigating a shear-thinning liquid (one for which the effective viscosity decreases as the shear

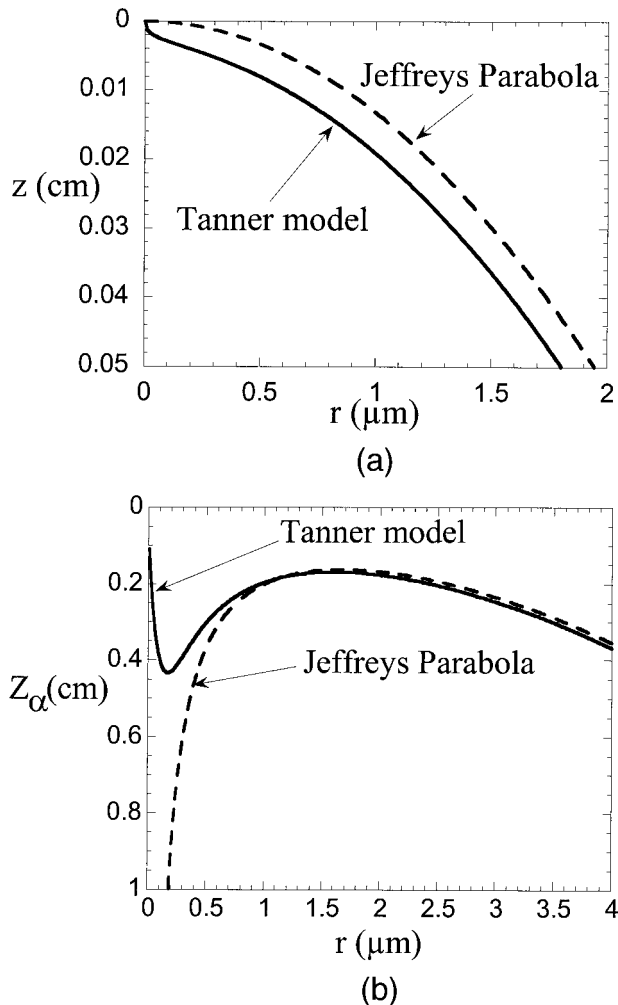


Fig. 10. (a) Theoretical profile of the liquid thin film including effects of surface tension; (b) predicted shape of the  $\alpha$  rainbow including effects of surface tension for  $\mu = 0.015 \text{ cm}^2/\text{s}$  and  $t = 20 \text{ s}$ .

rate increases) to see if TRM can be used to explore the fluid dynamics of a non-Newtonian thin film.

Near the top of the thin film, surface tension effects become important, and the Jeffreys parabola solution (which does not include them) is invalid. A model for the shape of a thin film that does include them is<sup>24</sup>

$$z = \left(\frac{g}{\mu}\right) r^2 t + k \left(\frac{\sigma r}{\rho g}\right)^{1/3}. \quad (18)$$

Here  $\sigma$  is the surface tension of the fluid,  $\rho$  is the fluid density, and  $k = 0.477$  is a dimensionless constant derived from fluid dynamics considerations. This model predicts that the film becomes vertical at the contact line  $r = 0$ . Realistically, the slope should approach the contact line with a small but nonzero value (the contact angle) determined by the free energy of the liquid–solid–air interface.<sup>26</sup> The silicone oils used in the experiments of Section 4 had  $\sigma = 20 \text{ dyn/cm}$  and  $\rho = 0.97 \text{ g/cm}^3$  for all values

of the viscosity. (At this point, we should mention that the Tanner model of Ref. 24 is derived for a flat plate. Because the radius of the rod we are using is comparable to  $L_\sigma = (\sigma/\rho g)^{1/2} = 1.4 \text{ mm}$ , the Tanner model may not adequately represent the true shape of the thin film on our rod.) Figure 10(a) shows the theoretical profile for a fluid with kinematic viscosity  $\mu = 0.015 \text{ cm}^2/\text{s}$  at a time  $t = 20 \text{ s}$  by use of this model. Note that the shapes of the film predicted by each model are nearly identical except for the region  $z < 0.002 \text{ cm}$  (corresponding to  $r < 0.05 \text{ }\mu\text{m}$ ) where the Jeffreys parabola intersects the rod perpendicularly, whereas the Tanner model intersects tangentially. The predicted  $Z$  coordinate of the  $\alpha$  rainbow on the viewing screen as a function of film thickness with Tanner’s model can be found from Eqs. (10) and (18) and is shown in Fig. 10(b). Although the change in the shape of the film profile is almost unnoticeable between the Tanner model and the Jeffreys parabola, the change in the shape of the rainbow is profound. This is because there is a second zero of  $dZ_{\alpha,\beta}/dr$ . Instead of shooting off to infinity as  $r \rightarrow 0$ ,  $Z_{\alpha,\beta}(r)$  goes through a maximum and returns to zero.

We believe that the true shape of the rainbow does look like that in Fig. 10(b). It is difficult to observe this as the rainbow that is due to this short section of the film is dim. Little of the incoming light is spread over a large vertical distance. However, by removing the cylindrical lens and focusing all the power in the laser beam at the point of attachment, we observed this branch of the rainbow. A simple theory predicts that this second gap width should narrow as  $t^{-2/5}$ . We are currently attempting to measure the spacing of the second gap as a function of time; the results of this research will be reported in a future publication.

Whether we can detect the effects of surface tension in measurements made below the region where surface tension effects dominate is unclear. For example, the effects of surface tension subtly change the gap width in the region of the film examined in Section 4. A perturbation theory expansion indicates that the gap width of Eq. (12) is increased by the additive term

$$\Delta Z_{\alpha,\beta}^0 = \frac{2}{3} \left(1 + \frac{R}{L_f}\right)^{8/9} k L_\sigma^{2/3} \left(\frac{\gamma_{\alpha,\beta} R \mu^2}{4g^2}\right)^{1/9} t^{-2/9}. \quad (19)$$

Unfortunately, a scaling law of  $t^{-29}$  is difficult to distinguish from the scaling law of  $t^{-13}$  in Eq. (12). Also, the contribution this makes to the gap width is only of the order of 1% of the total gap width and approximately 10% of the constant offset  $B_{\alpha,\beta}$  of Eq. (13). This means that its contribution is of the order of the resolution of the camera that we are currently using. If this subtle effect is measurable, it will be most important in measurements made on low-viscosity fluids at long times. We have not been able to measure this effect yet for reasons discussed below.

It is possible to determine the position of the contact line (the point where the film joins the rod) to an

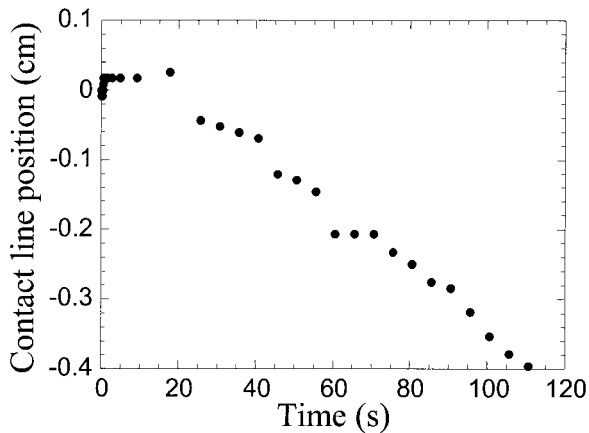


Fig. 11. Contact line position as a function of time for  $\mu = 0.015 \text{ cm}^2/\text{s}$ .

accuracy of approximately  $10 \text{ }\mu\text{m}$  with TRM. It is the top of the rainbow gap in Fig. 4. For the lowest-viscosity fluid examined, we found that, after approximately 1 min, the contact line began to slip down the rod. Figure 11 shows a graph of the contact line motion over time. As can be seen, it does not slip steadily, but sticks irregularly as it descends. If this is actually the case, it represents a macroscopic violation of the no-slip boundary condition of fluid mechanics. These results are not confirmed, however, because the lowest-viscosity fluids are more volatile than the higher-viscosity fluids, and we need to rule out evaporation as the cause of this apparent motion. We do not believe that evaporation is the cause, as we have also investigated TRM using highly volatile liquids such as methanol, and the results of these experiments appear completely different than what we see in Fig. 11, but the possibility is still open.

### Appendix A

Consider a circular cylinder of radius  $a$  and refractive index  $n_1$  whose symmetry axis coincides with the  $z$  axis of an  $x,y,z$  rectangular coordinate system. The cylinder is coated with a liquid of refractive index  $n_2$  whose thickness tapers as  $r(z)$ . For the Jeffreys parabola,

$$r(z) = \left( \frac{\mu z}{gt} \right)^{1/2}, \quad (\text{A1})$$

as in Eq. (9). A light ray whose trajectory is initially confined to the  $x,y$  plane approaches the cylinder parallel to the  $x$  axis. In this appendix we calculate the trajectory of the ray making one internal reflection at either the cylinder-coating interface or the coating-air interface before exiting the coated cylinder and propagating to the scattering far zone using the analytical ray-tracing method described in Ref. 27.

The incident ray intersects the coating surface at point  $O$ . Let  $\psi_0$  be the angle in the  $x,y$  plane that the vector from the cylinder axis to point  $O$  makes with the  $-x$  axis. The quantity  $[a \sin(\psi_0)]$  is commonly

called the impact parameter of the incident ray. The inward normal to the coating surface at point  $O$  is

$$\mathbf{n}_0 = \cos(\gamma)\cos(\psi_0)\mathbf{u}_x - \cos(\gamma)\sin(\psi_0)\mathbf{u}_y + \sin(\gamma)\mathbf{u}_z, \quad (\text{A2})$$

where  $\gamma$  is the angle the coating surface makes with the  $z$  axis at point  $O$ , i.e.,

$$\tan \gamma = \left. \frac{dr}{dz} \right|_0. \quad (\text{A3})$$

We assume that the surface of the coating is nearly vertical so that  $\gamma \ll 1$  and the coating is always of negligible thickness compared to the cylinder radius. We take the incident ray to be the first-order rainbow ray of the cylinder in the absence of the coating so that

$$\cos \psi_0 = \left( \frac{n_1^2 - 1}{3} \right)^{1/2}, \quad \sin \psi_0 = \left( \frac{4 - n_1^2}{3} \right)^{1/2} \quad (\text{A4})$$

and assume that propagation through the coating does not substantially change the impact parameter of the rainbow ray from that of Eqs. (A4). The trajectory of a ray diagonally incident on a circular cylinder can be decomposed into a trajectory in the  $x,y$  plane as can be seen from above by use of the Bravais refractive index of the cylinder and a vertical trajectory as can be seen from the side by use of the cylinder's actual refractive index.<sup>28</sup> In like manner, we similarly decompose the trajectory of a ray horizontally incident on a circular cylinder with a tapered coating.

As the initially horizontal ray refracts from the air into the coating, it deflects vertically by an angle

$$\xi \approx \frac{[(n_2^2 - \sin^2 \psi_0)^{1/2} - \cos \psi_0]\gamma}{n_2}. \quad (\text{A5})$$

Because the coating is of negligible thickness, we can neglect the presence of the coating when examining the trajectory of the ray in the  $x,y$  plane, and, because  $\gamma \ll 1$ , the Bravais refractive index of the cylinder is nearly the same as its actual refractive index. As a result, the  $x,y$  trajectory of the ray as seen from above is nearly identical to that of a horizontal ray incident on an uncoated cylinder. At point 1 in Fig. 1, the ray is vertically deflected by the angle  $\eta$  with respect to the horizontal where

$$n_1 \sin \eta = n_2 \sin \xi. \quad (\text{A6})$$

The  $\beta$  ray of Fig. 1 is then transmitted from the cylinder to the coating at point 2 in Fig. 1, it internally reflects from the coating-air interface at point 3, is transmitted back into the cylinder at point 4, is transmitted back into the coating at point 5, and finally refracts from the coating to the air at point 6. Although the ray continues to rise vertically throughout its trajectory, we assume that  $r(z)$  is a relatively slowly varying function so that the angle the coating surface makes with the  $z$  axis at points 0,3, and 6 is nearly identical. This assumption is quite accurate

for the Jeffreys parabola far from the contact line. The angle the ray makes with respect to the  $x,y$  plane in the coating between points 2 and 3 is again  $\zeta'$ , and after internal reflection by the tilted interface at point 3, the ray makes the angle

$$\xi_3 \approx \xi + \frac{2\gamma}{n_2} (n_2^2 - \sin^2 \psi_0)^{1/2} \quad (\text{A7})$$

with the  $x,y$  plane. After the ray is transmitted back into the cylinder at point 4, it makes an angle  $\eta_3$  with respect to the  $x,y$  plane where

$$n_1 \sin \eta_3 = n_2 \sin \xi_3, \quad (\text{A8})$$

and when back in the coating between points 5 and 6, it again makes the angle  $\xi_3$  with respect to the vertical. After refraction back into the air, the exiting ray makes the angle

$$\begin{aligned} \xi_6 &\approx n_2 \xi_3 - \gamma [\cos \psi_0 - (n_2^2 - \sin^2 \psi_0)^{1/2}] \\ &= \frac{2\gamma}{3^{1/2}} [2(3n_2^2 + n_1^2 - 4)^{1/2} - (n_1^2 - 1)^{1/2}], \quad (\text{A9}) \end{aligned}$$

which is equivalent to Eq. (11b).

The  $\alpha$  ray, on the other hand, internally reflects from the vertical cylinder–coating interface at point 2' in Fig. 1 with the angle  $\eta$  with respect to the vertical, is transmitted back into the coating at point 3', and refracts out of the coating into the air at point 4'. When in the coating between points 3' and 4', the ray again makes an angle  $\xi$  with respect to the  $x,y$  plane; and after refraction into the air, the exiting ray makes the angle

$$\begin{aligned} \xi_4' &\approx n_2 \xi - \gamma [\cos \psi_0 - (n_2^2 - \sin^2 \psi_0)^{1/2}] \\ &= \frac{2\gamma}{3^{1/2}} [(3n_2^2 + n_1^2 - 4)^{1/2} - (n_1^2 - 1)^{1/2}] \quad (\text{A10}) \end{aligned}$$

with the  $x,y$  plane, which is equivalent to Eq (11a).

If the height of the incident ray above the contact line at point  $O$  is  $z$ , the height  $Z_{\alpha,\beta}$  where the far-zone scattered  $\alpha$  or  $\beta$  rainbow ray intersects the viewing screen a distance  $R$  from the cylinder axis is

$$Z_{\alpha,\beta} = z + d + (R - \alpha)\xi_{\alpha,\beta}, \quad (\text{A11})$$

where  $\xi_\alpha = \xi_4'$ ,  $\xi_\beta = \xi_6$ , and  $d < 4\alpha\eta$ . The  $d$  term is ignored because  $\eta$  is assumed to be small. Last, consider the case in which the family of incident rays is not initially horizontally propagating. Rather, the ray family is a diverging laser beam that has been passed through a cylindrical lens of focal length  $f$ . In this case, for a ray in the family initially making the angle  $\delta$  with the  $x,y$  plane and arriving at point  $O$  at the height  $z$ , the ray-tracing calculation through the coated cylinder proceeds as before. In approximations (A9) and (A10) the exiting angles  $\xi_6$  and  $\xi_4'$  are each increased by  $\delta$ , and Eq. (A11) becomes

$$Z_{\alpha,\beta} = z + \frac{(R - \alpha)(z - z_c)}{f} + (R - \alpha)\xi_{\alpha,\beta}, \quad (\text{A12})$$

where  $z_c$  is the height of the center of the diverging beam. Equation (A12) is equivalent to Eq. (10).

This research was supported in part by National Science Foundation grant PHY-9987862 and by NASA grants NCC3-909 and NAG3-2774. We thank Andy Koch and Darlene Vangaasbeck for help with cleaning our glass rods and Ivan Sterling for help with numerically integrating Eq. (14).

## References

1. C. W. Chan and W. K. Lee, "Measurement of a liquid refractive index by using high-order rainbows," *J. Opt. Soc. Am. B* **13**, 532–535 (1996).
2. H. Hattori, H. Yamanaka, H. Kurniawan, S. Yokoi, and K. Kagawa, "Using minimum deviation of a secondary rainbow and its application to water analysis in a high-precision, refractive-index comparator for liquids," *Appl. Opt.* **36**, 5552–5556 (1997).
3. H. Hattori, H. Kakui, H. Kurniawan, and K. Kagawa, "Liquid refractometry by the rainbow method," *Appl. Opt.* **37**, 4123–4129 (1998).
4. H. Hattori, "Simulation study on refractometry by the rainbow method," *Appl. Opt.* **38**, 4037–4046 (1999).
5. J. Hom and N. Chigier, "Rainbow refractometry: simultaneous measurement of temperature, refractive index, and size of droplets," *Appl. Opt.* **41**, 1899–1907 (2002).
6. C. L. Adler, J. A. Lock, and B. R. Stone, "Rainbow scattering by a cylinder with a nearly elliptical cross section," *Appl. Opt.* **37**, 1540–1550 (1998).
7. C. L. Adler, J. A. Lock, D. Phipps, K. Saunders, and J. Nash, "Supernumerary spacings of rainbows produced by an elliptical cross-section cylinder. II: Experiment," *Appl. Opt.* **40**, 2535–2545 (2001).
8. H. M. Nussenzweig, "Complex angular momentum theory of the rainbow and the glory," *J. Opt. Soc. Am.* **69**, 1068–1079 (1979).
9. T. Nousiainen, "Scattering of light by raindrops with single-mode oscillations," *J. Atmos. Sci.* **57**, 789–802 (2000).
10. T. Nousiainen and K. Muinonen, "Light scattering by Gaussian randomly oscillating raindrops," *J. Quant. Spectrosc. Radiat. Transfer* **63**, 643–666 (1999).
11. J. P. A. J. van Beeck, D. Giannoulis, L. Zimmer, and M. L. Riethmuller, "Global rainbow thermometry for droplet-temperature measurement," *Opt. Lett.* **24**, 1696–1698 (1999).
12. P. L. Marston, "Catastrophe optics of spheroidal drops and generalized rainbows," *J. Quant. Spectrosc. Radiat. Transfer* **63**, 341–351 (1999).
13. C. L. Adler, J. A. Lock, J. K. Nash, and K. W. Saunders, "Experimental observation of rainbow scattering by a coated cylinder: twin primary rainbows and thin-film interference," *Appl. Opt.* **40**, 1548–1558 (2001).
14. J. A. Lock, J. M. Jamison, and C.-Y. Lin, "Rainbow scattering by a coated sphere," *Appl. Opt.* **33**, 4677–4691 (1994).
15. A. L. Aden and M. Kerker, "Scattering of electromagnetic waves from two concentric spheres," *J. Appl. Phys.* **22**, 1242–1246 (1951).
16. G. B. Airy, "On the intensity of light in the neighbourhood of a caustic," *Trans. Cambridge Philos. Soc.* **6**, 397–403 (1836).
17. R. Greenler, *Rainbows, Halos and Glories* (Cambridge U. Press, Cambridge, UK, 1980), pp. 8–10.
18. M. Minnaert, *Light and Color in the Outdoors* (Springer-Verlag, New York, 1993), pp. 195–197.
19. H. M. Nussenzweig, "The theory of the rainbow," *Sci. Am.* **236**, 116–127 (1977).

20. H. C. van de Hulst, *Light Scattering by Small Particles* (Wiley, New York, 1957), pp. 240–246.
21. M. Abramowitz and I. A. Stegun, eds., *Handbook of Mathematical Functions* (Dover, New York, 1970), p. 478.
22. H. Jeffreys, “The drainage of a vertical plate,” *Proc. Cambridge Philos. Soc.* **26**, 204–205 (1930).
23. C. Gutfinger and J. A. Tallmadge, “Some remarks on the problem of drainage of fluids on vertical surfaces,” *AIChE. J.* **10**, 774–780 (1964).
24. L. H. Tanner, “The form and motion of draining oil drops,” *J. Phys. D* **18**, 1311–1326 (1985).
25. D. Ramakrishna and N. Ch. Pattabhiramacharyulu, “Dusty viscous drainage on a vertical cylinder,” *Proc. Indian Acad. Sci. Sect. A* **53**, 257–266 (1987).
26. P. C. Hiemenz, *Principles of Colloid and Surface Chemistry*, 2nd. ed. (Marcel Dekker, New York, 1986), pp. 287–299.
27. J. B. Keller and H. B. Keller, “Determination of reflected and transmitted fields by geometrical optics,” *J. Opt. Soc. Am.* **40**, 48–52 (1950), Appendix 1.
28. C. L. Adler, J. A. Lock, B. R. Stone, and C. J. Garcia, “High-order interior caustics produced in scattering of a diagonally incident plane wave by a circular cylinder,” *J. Opt. Soc. Am. A* **14**, 1305–1315 (1997).